Eur. Phys. J. D **19**, 79–87 (2002)
DOI: 10.1140/epjd/e20020058

THE EUROPEAN PHYSICAL JOURNAL D
EDP Sciences

Ionization waves: from stability to chaos and turbulence

A. Atipo[1], G. Bonhomme[1,a], and T. Pierre[2]

[1] Laboratoire de Physique des Milieux Ionisés et Applications[b], Université Henri Poincaré, B.P. 239, 54506 Vandœuvre-lès-Nancy Cedex, France
[2] Laboratoire PIIM[c], Université de Provence, 13397 Marseille Cedex 20, France

Received 25 October 2001

Abstract. The spatio-temporal dynamics of self-excited ionization waves in a neon glow discharge is experimentally investigated. Various mechanisms leading to ionization waves chaos and turbulence are identified: subharmonics cascade, Ruelle-Takens-Newhouse scenario, and spatio-temporal intermittency. The dynamical states involved in the transition scenarios from stability to chaotic regimes are characterized through both temporal and spatio-temporal analysis by means of the Biorthogonal Decomposition (BD).

PACS. 52.35.Mw Nonlinear phenomena: waves, wave propagation, and other interactions (including parametric effects, mode coupling, ponderomotive effects, etc.) – 52.80.Hc Glow; corona – 05.45.-a Nonlinear dynamics and nonlinear dynamical systems

1 Introduction

Most spatially extended dissipative systems exhibit complex nonlinear spatio-temporal dynamics, leading to pattern formation, spatiotemporal chaos or turbulence [1]. The understanding of this dynamics is a challenging problem. Among these systems, glow discharges exhibit rich dynamical behaviours and are easily investigated using optical diagnostics. Moreover, they are an adequate system for modeling the spatiotemporal dynamics.

This rich dynamical behavior of the discharge is due – as it has been long known [2–6] – to the nonlinear interaction of ionization waves propagating along the plasma column. In this paper, we report on a detailed description of the various mechanisms of transition towards chaos and turbulence observed in a glow discharge in neon. In order to understand the role of spatiotemporal coherent structures in the appearance of complex regimes, a spatiotemporal analysis is performed using the Biorthogonal Decomposition (BD) [7]. This method allows to investigate the different regimes beside the characterization of the nonlinear temporal dynamics using the classical tools such as correlation and information dimensions, and Lyapunov exponents computed for phase space trajectories reconstructed from experimental time-series.

The paper is organized as follows. In Section 2, details concerning the experimental set-up and the analysis tools are given. Then, in the next section, we describe the experimentally observed transition scenarios towards chaos and turbulence and characterize the dynamical regimes. In Section 4, we discuss how the discharge evolves from a compact low dimensional system to an extended system by changing the length of the plasma column.

2 Experiments and numerical analysis tools

The experiment is carried out in conventional discharge tubes filled with flowing neon gas (1 to 5 torrs). A discharge tube of 4.8 cm in diameter, 50 cm in length generates a fixed length discharge, and a long tube of 3 cm in diameter, 100 cm in length, with one movable electrode allows the variation of the discharge length. The discharge voltage and current can be varied from 300 to 1 000 V and from 0 to 100 mA, respectively. The detection of the ionization waves propagating in the plasma column is made using an array of collimated photo-detectors. Each detector is probing a section of the column of 8 mm width. The axial separation between the detectors is 10 or 15 mm. The typical wavelength of the propagating waves is 8 cm corresponding to 6 to 8 sampling points in one wavelength. The crucial point in spatiotemporal investigations is to record data simultaneously at different locations of the system. In our case, three fast 16-channels digitizers (VXI plug-in units,Tektronix VX4244) are used for performing the synchronous acquisition of the signals emanating from 16 up to 48 photo-diodes. The 200 kHz sampling rate and 16-bits resolution of the digitizer allow for reliable long time-series (64 ksamples/channel). Digitized signals are then stored in a computer for the display of the various spatiotemporal regimes and real-time processing.

[a] e-mail: Gerard.Bonhomme@lpmi.uhp-nancy.fr
[b] UMR 7040 du CNRS
[c] UMR 6633 du CNRS

Being available a set of M time-series simultaneously measured at M different locations x_j of the discharge, the spatiotemporal analysis can be done either by the determination of a set of local characteristics through the time-series analysis or by the global analysis of the space-time data $Y_{ij} = Y(x_j, t_i)$ formed by the M time-series, after mean substracting and normalizing, *i.e.*, $(Y(x_j, t_i) = (y_j(t_i) - \overline{y_j})/\sigma_j$, with $i = 1, 2, ..., N$.

The former analysis consists, after the reconstruction of phase-space portraits either with the delay method or by using the singular value decomposition [11,12], in performing the calculation of dimensions and Lyapunov spectra [13–15].

Space-time dynamics is characterized from inspection of space-time and space-frequency plots, and by means of the biorthogonal decomposition (BD) of the space-time signal $Y(x_j, t_i)$. The BD [7] expands a signal $Y(x, t)$ in a weighted sum of spatial and temporal eigenfunctions $\Phi_k(x)$ and $\Psi_k(t)$ called *topos* and *chronos* respectively. These eigenfunctions come out from the numerical analysis and are not imposed from outside as in Fourier decomposition. Among all linear decompositions, the BD is the most efficient in the sense of capturing the most energy possible on a given number of modes [8] and has proven to be a very convenient tool for analyzing two-dimensional data [7,9,10]. In the case of discrete data the BD is simply given by the singular value decomposition of the rectangular matrix associated to the space-time signal which can be expressed in the form:

$$Y_{ij} = \sum_{k=1}^{K} \alpha_k \Psi_k(t_i) \Phi_k(x_j) \qquad (1)$$

where α_k, Ψ_k, Φ_k are the *weights*, *chronos* and *topos*, respectively, with the orthogonality property:

$$(\Phi_i, \Phi_j) = (\Psi_i, \Psi_j) = \delta_{ij}.$$

Equal weights (degeneracy) correspond to space-time symmetries. It is the case for example for travelling waves (*i.e.*, two equal weights); the two chronos and the two topos corresponding to the equal weights have the same spectral components and build a propagating structure. A single weight corresponds to a non-propagating structure. Making a partial reconstruction from the weighted sum of spatial and temporal eigenfunctions gives a mean to extract coherent structures from the background stochastic fluctuations.

The distribution of weights gives a measure for the spatio-temporal complexity. In particular we can construct the quantity $D_{\mathrm{BD}}(K)$ defined by:

$$D_{\mathrm{BD}}(K) = \exp\left\{ -\sum_{k=1}^{K} p_k \ln p_k \right\} \qquad (2)$$

where $p_k = \alpha_k^2 / \sum \alpha_k^2$.

It can give the number of terms needed in the weighted sum above and that adequately represent the space-time signal $Y(x_j, t_i)$. This number corresponds to the number L where the quantity $D_{\mathrm{BD}}(K)$ possibly saturates with increasing K.

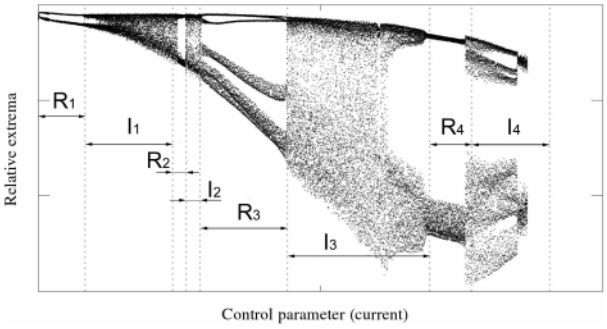

Fig. 1. Experimental bifurcation diagram.

3 Transitions from regular to irregular motion and spatiotemporal analysis

At pressures under consideration here, ionization waves can exhibit regular, chaotic or turbulent behaviour depending on the discharge current.

For a sake of simplification, the transition scenarios are investigated for a fixed length of the discharge (4.8 cm in diameter and 50 cm in length, the length of the positive column being about 34 cm) at a pressure of 3 torrs ($pR = 7.2$ cm torr). Starting from null current and increasing the discharge current results in an increase of the light emission along the positive column correlated with an increase of the ionization waves amplitude. A value of the current is then obtained – depending on the neon pressure – where the amplitude of the signals begins to decrease. At higher discharge current, the ionization waves completely disappear and the discharge becomes homogeneous. The high current limit of the excitation domain of ionization waves is known as the Pupp limit [2]. It depends on the gas pressure.

By plotting the maxima and the minima of the light intensity recorded at a fixed location along the positive column as the discharge current is varied, the bifurcation diagram qualitatively describing the ionization waves dynamics is obtained. A typical bifurcation diagram obtained when the discharge current is continuously and slowly decreased from 60 to 0 mA is displayed in Figure 1. The variation rate of the discharge current is 60 mA/s. The bifurcation diagram depicted in Figure 1 is issued from a long time-series recorded in a section of the discharge located 1 cm from the anode. The intervals where the dynamics is regular (branches) can be clearly distinguished from the irregular ones (scatter plot). On the bifurcation diagram, the regular and irregular regimes are referred to as R_m et I_n, respectively, where m and n are indexes.

The value of the current corresponding to boundaries of each of these intervals are given in Table 1. Let us underline however that, because of the hysteresis phenomenon, the current limits corresponding to each regime vary in a more or less significant way. Two different current sweepings lead for the same tube parameters to slightly different current intervals. The higher current limit, where the amplitude of the ionization waves vanished, is not on the bifurcation diagram. The reason is that arcs are generated

Table 1. Current ranges corresponding to regular and irregular regimes in the bifurcation diagram.

Regular regimes	R_1	R_2	R_3	R_4
Current (mA)	9–14	21–23	24–30	40–60
Irregular regimes	I_1	I_2	I_3	I_4
Current (mA)	14–21	23–24	30–40	60–...

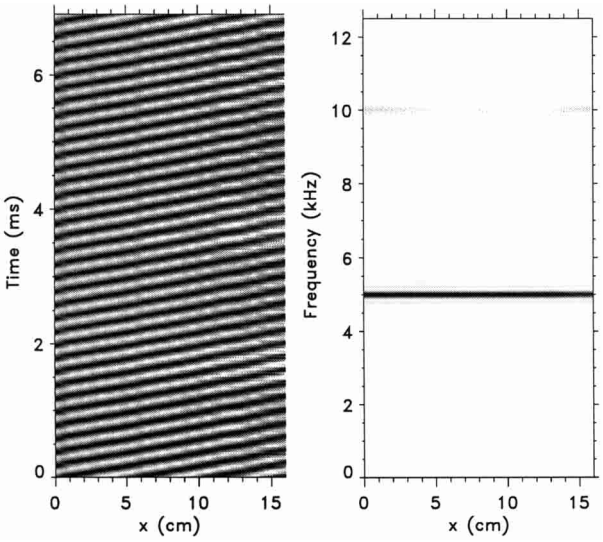

Fig. 2. Space-time and space-frequency plots, $I = 93$ mA.

in the discharge at high current and prevent from continuously varying the current up to this limit. Nevertheless a very slow variation makes it possible to reach this high current limit, while keeping a stable plasma.

It is necessary to examine carefully the transition from the regular regime towards the irregular regime in order to understand the route towards chaos. Different cases have to be considered depending on the distance to the high current limit corresponding to the stable homogeneous plasma.

3.1 High current limit

Starting from this stationary regime and crossing the Pupp limit by decreasing the discharge current, a limit cycle regime with frequency $f_1 \approx 5$ kHz appears all along the whole positive column. It corresponds to a single coherent travelling wave with wavelength $\lambda \approx 5$ cm. A further decrease of the discharge current leads to high periodicity regimes by sub-harmonics cascade. Then, the broadband spectrum associated to the chaotic regimes occurs. A typical situation of a sub-harmonics cascade obtained at a pressure of 3 torrs is given in Figures 2 to 5. The smoothed space-time data as well as the corresponding space-frequency diagrams are shown in these figures. The first regime depicted in Figure 2 is a limit cycle regime with a frequency $f_1 = 5.27$ kHz ($I = 93$ mA). The second (Fig. 3) is a period-3 regime with the presence of the frequency f_1 (slightly decreased to $f_1 = 4.64$ kHz) and its sub-harmonics $f_1/3 = 1.76$ kHz and $2f_1/3 = 3.52$ kHz.

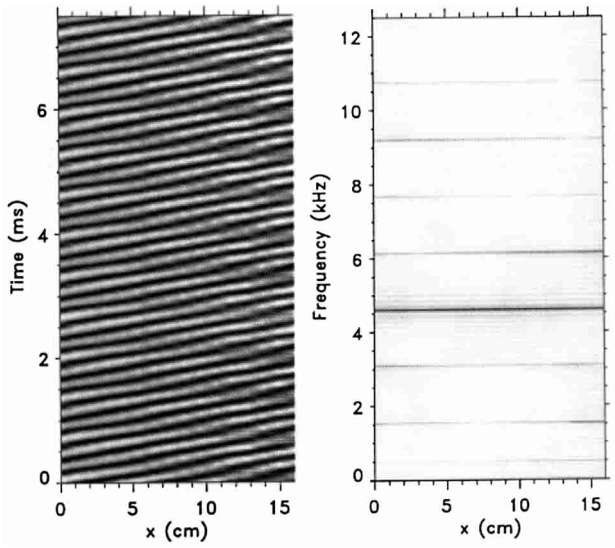

Fig. 3. Space-time and space-frequency plots, $I = 90$ mA.

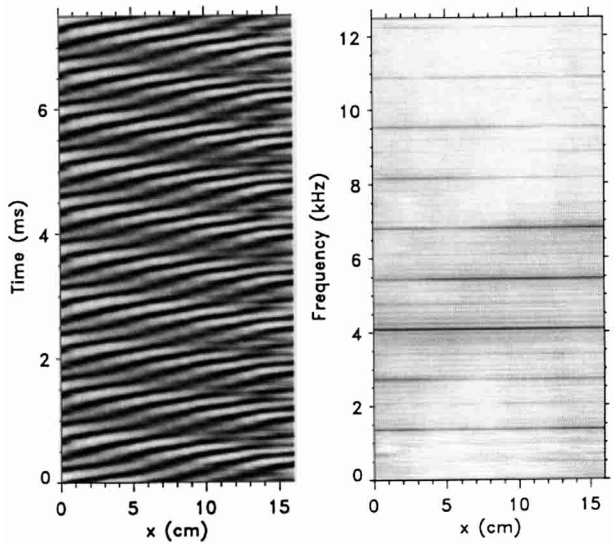

Fig. 4. Space-time and space-frequency plots, $I = 87$ mA.

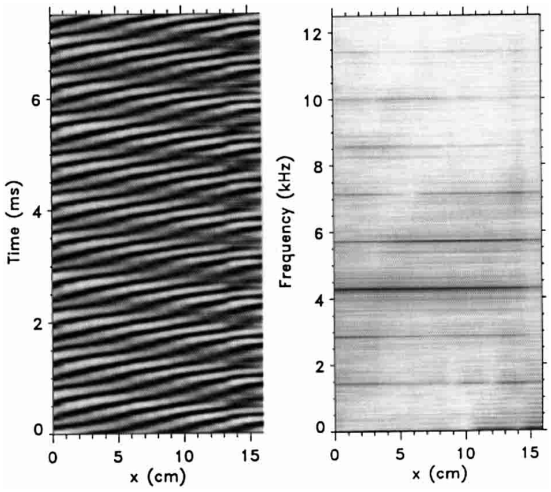

Fig. 5. Space-time and space-frequency plots, $I = 82$ mA.

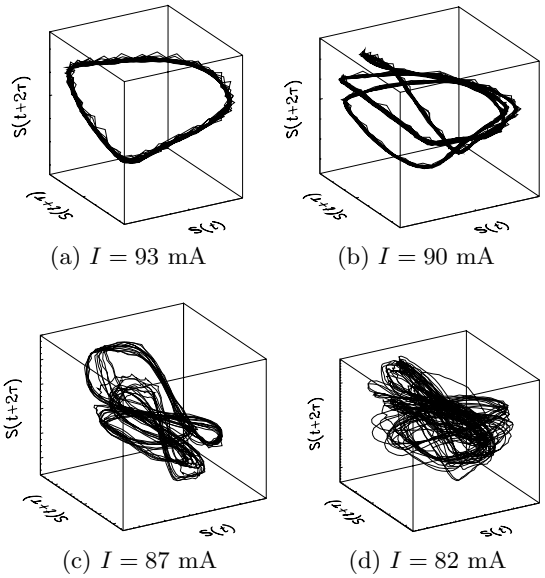

(a) $I = 93$ mA (b) $I = 90$ mA

(c) $I = 87$ mA (d) $I = 82$ mA

Fig. 6. Phase portraits reconstructed from time-series taken near the anode end for each of the regimes depicted in Figures 2 to 5.

Table 2. Fundamental wave properties and dynamical characteristics for the subharmonics scenario. D_2: correlation dimension, λ_i: Lyapunov exponents in descending order.

Regime	I (mA)	f (kHz)	λ (cm)	D_2	λ_i
period-1	93	5.27	4.5	1.0	0, –, –, ...
period-3	90	4.64	4.65	1.0	0, –, –, ...
high periodicity	87	4.3	5	1.0	0, –, –, ...
chaos	82	4.3	5	2.8	+, 0, –, –, ...

The third regime (Fig. 4) is of higher periodicity and the last (Fig. 5) is a chaotic regime.

The results of the analysis of time-series extracted from the space-time data shown in Figures 2 to 5 are given in Table 2. For each space-time data one time-series picked up at 1 cm from the anode has been analyzed. The associated phase space trajectories, reconstructed by the time delay method, are plotted in Figure 6.

It is interesting to examine the spatiotemporal behaviour from the results of the biorthogonal decomposition of the space-time data shown in Figures 2 to 5. The evolution of the quantity $D_{\mathrm{BD}}(K)$ (Fig. 7b) for the four regimes show that the spatial structure is made up of a few modes even in the case of the chaotic regime. The saturation of these quantities starting from a small value of K indicates that the spatiotemporal information contained in the analyzed signals can be concentrated on a few modes associated with the most dominating coefficients. The other coefficients are associated with the stochastic fluctuations. For each regime, the weights distribution exhibits two dominating weights (α_1, α_2) building a travelling wave of frequency f_1 which represents the fundamental ionization wave. One observes in Figure 7a

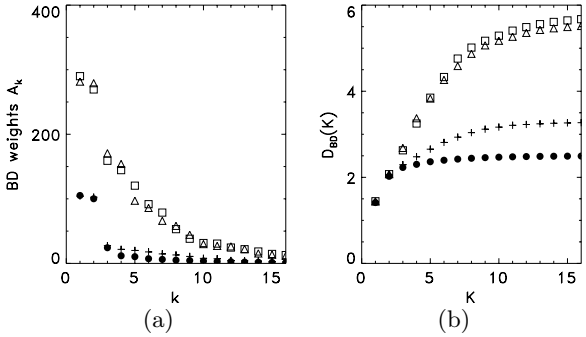

(a) (b)

Fig. 7. The BD results for: limit cycle (•), period-3 (+), period-6 (△), and chaotic (□) regimes; (a) weights distribution, (b) $D_{\mathrm{BD}}(K)$.

the stability of this fundamental mode during the transition towards chaos, since the amplitude of the weights α_1 and α_2 remains unchanged when switching from a regime to another. The reconstruction of this fundamental ionization wave for each of the four analyzed regimes are represented in Figure 8. The space-time structure of this mode is practically unchanged during the transition towards chaos. The harmonics of the fundamental mode are associated to the next couples of dominating coefficients (α_3, α_4) and (α_5, α_6). These latter modes degenerate during the transition towards chaos. Their space-time structures become much more complex and deviate from the space-time structures of simple harmonics, making it difficult to reconstruct their space-time structures with only sixteen detectors as it is the case. The fundamental ionization wave is the only mode present near the Pupp limit. Then, the non linear excitation of sub-harmonics leads to the sub-harmonics bifurcation scenario.

3.2 Intermediate currents

Beside the limit cycle regime obtained at a discharge current slightly lower than the Pupp limit – whose destabilization scenario has been discussed above – the regular regimes observed in the discharge are most often destabilized following the Ruelle, Takens and Newhouse (RTN) scenario, *i.e.*, a quasi-periodic state which builds up from two interacting modes with incommensurate frequencies becomes gradually chaotic, with the variation of the discharge current.

The spatiotemporal signals corresponding to the regimes exhibiting such a transition to chaos following this quasi-periodicity route are represented in Figures 9 to 12. The discharge current associated with these four regimes: periodic, quasi-periodic, chaotic and turbulent regimes is 40, 53, 76 and 79 mA, respectively. On each image, the anode is on the left and the cathode is on the right. For each of the four regimes, we have represented the phase portraits (Fig. 13) and determined the dynamical characteristics (Tabs. 3 and 4).

In contrast to the case of the sub-harmonics cascade discussed in the previous section, the initial limit cycle

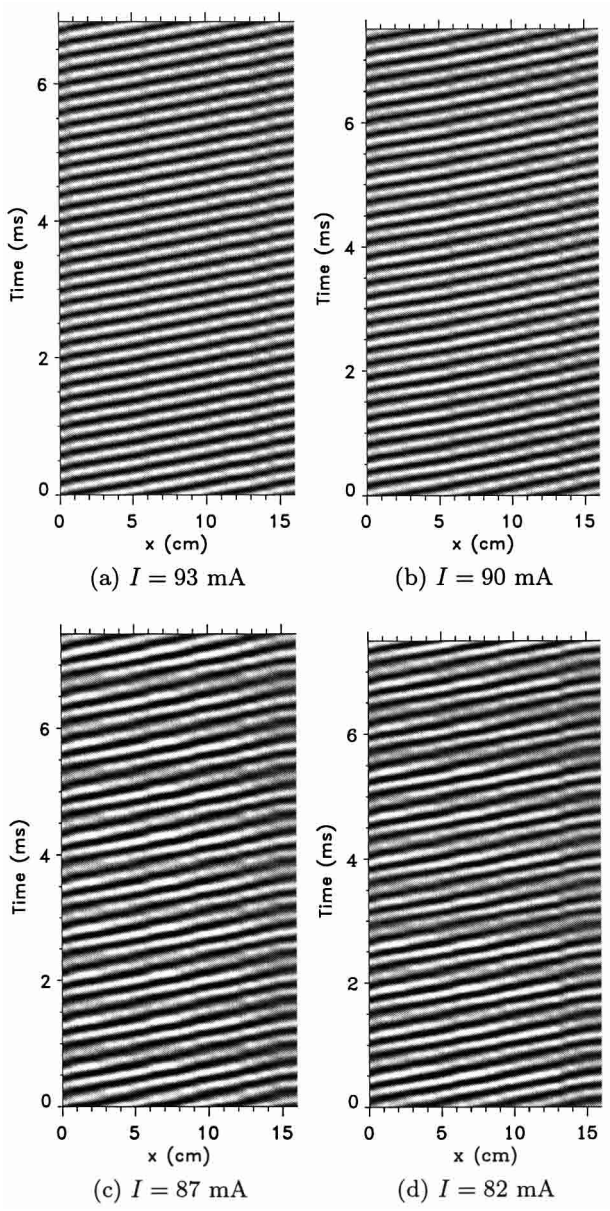

Fig. 8. Space-time dynamics of the dominant traveling wave reconstructed from the biorthogonal decomposition of space-time data, *i.e.*, $\sum_{k=1}^{2} \alpha_k \Psi_k(t_i)\Phi_k(x_j)$ from: (a) mono-chromatic, (b) period-3, (c) high periodicity, and (d) chaotic regimes.

regime looks quite different (see Fig. 9a).Whereas the frequency is the same all along the positive column in the suharmonics cascade, we observe now that the limit cycle ($I = 40$ mA) has a frequency $f_1 = 2.64$ kHz in the anodic part of the discharge and a frequency $f_c = 5.28$ kHz $\approx 2f_1$ in the cathodic part of the discharge. This reflects the existence of two different ionization modes: one dominating only near the cathode end, and the other dominating in most of the positive column.

This is clearly seen in the space-time plot (Fig. 9a) which shows transitions between different wave propagation behaviors from one end to the other. Near the anode

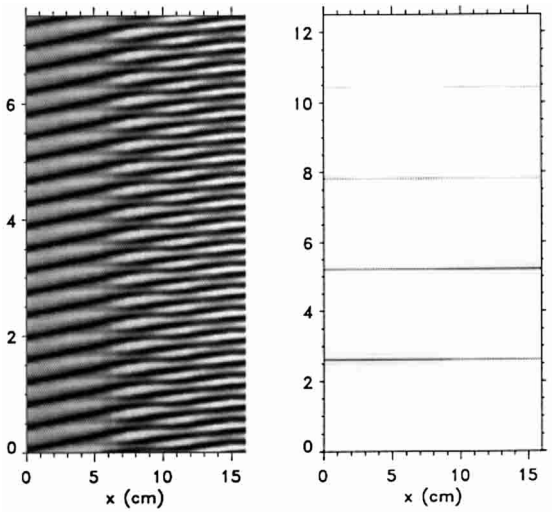

Fig. 9. Space-time and space-frequency plots, $I = 40$ mA.

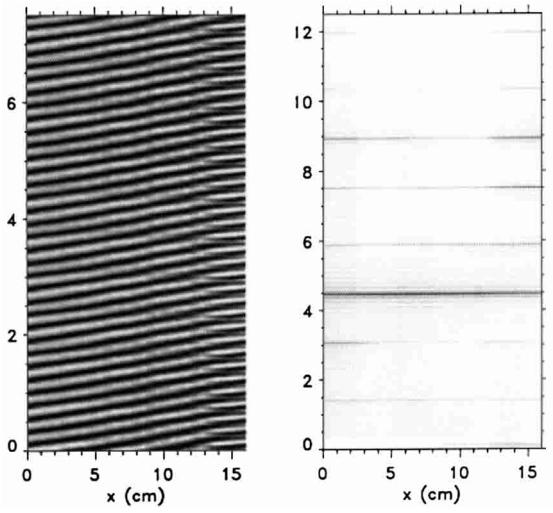

Fig. 10. Space-time and space-frequency plots, $I = 53$ mA.

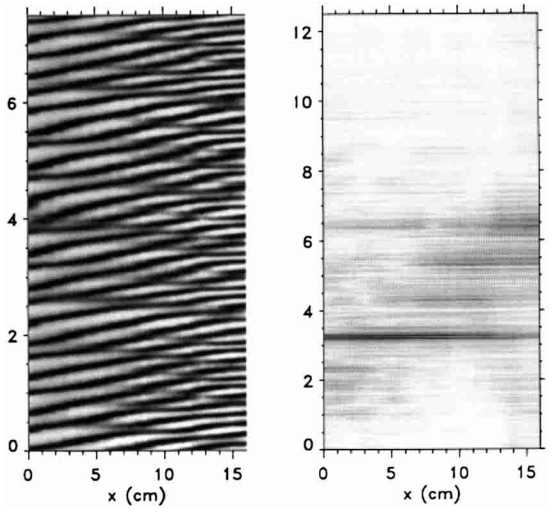

Fig. 11. Space-time and space-frequency plots, $I = 76$ mA.

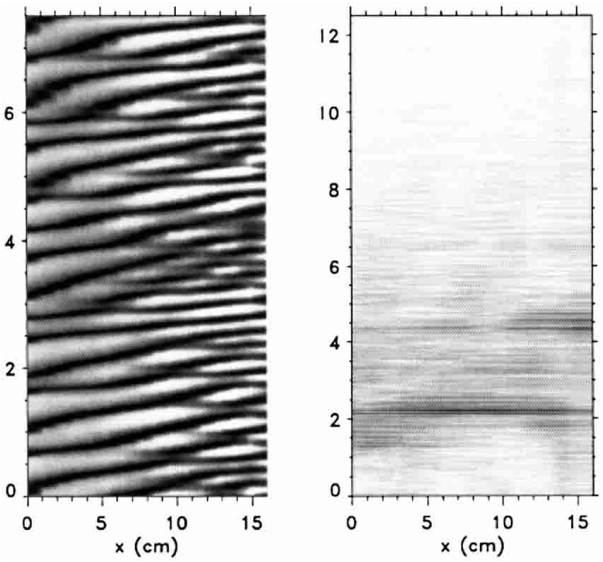

Fig. 12. Space-time and space-frequency plots, $I = 79$ mA.

Table 3. Waves properties and dynamical characteristics for the RTN scenario (anode side of the discharge).

Regime	I (mA)	f (kHz)	λ (cm)	D_2	λ_i
period-1	40	2.64	8.5	1.0	0, –, –, –, ...
QP	53	4.45	6	2	0, –, –, –, ...
chaotic	76	3.2	9	2.7	+, –, –, –, ...
turbulent	79	2.2	-	3.6	+, –, –, –, ...

Table 4. Waves properties and dynamical characteristics for the RTN scenario (cathode side of the discharge).

Regime	I (mA)	f (kHz)	λ (cm)	D_2	λ_i
period-2	40	5.28	17	1.0	0, –, –, –, ...
QP	53	4.45	6	2	+, –, –, –, ...
chaotic	76	6.4	3	2.9	+, –, –, –, ...
turbulent	79	-	-	-	+, +, 0, –, ...

the dominant mode is a travelling wave with wavelength $\lambda \approx 8.5$ cm and frequency f_1. Going toward the cathode end of the positive column, from some location arises a more complex space-time pattern corresponding to the interaction between the former wave and a second one with wavelength $\lambda \approx 17$ cm and frequency f_c. The properties of these two waves are indeed in agreement with the well known anomalous dispersive properties of the so-called p-waves, well described by a $\omega k = c^{st}$ law. The interaction between these two modes of frequencies f_1 and $f_c \approx 2f_1$ explains the period-2 regime seen in the phase portrait (Fig. 13b) as well.

The onset of the quasi-periodic regime is clearly associated to a variation of the frequency shift between the two modes as the current increases from 40 mA to 53 mA. The decreased frequency ($f_c \approx 4.5$ kHz) of the second mode becomes incommensurate with the first frequency

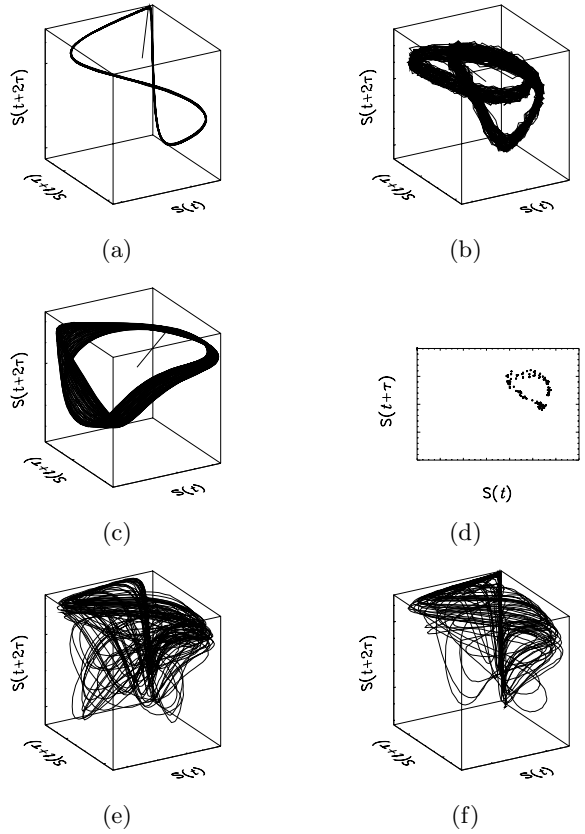

Fig. 13. Phase portraits reconstructed from time-series taken near the anode, except case (b), for each of the regimes depicted in Figures 9 to 12. (a) $I = 40$ mA, (anode), (b) $I = 40$ mA, (cathode), (c) $I = 53$ mA, (d) Poincaré section of attractor plotted in (c), (e) $I = 76$ mA, (f) $I = 79$ mA.

f_1, this latter being slightly increased up to $f_1 = 2.9$ kHz, for this current.

On the anode side the dynamical characteristics and phase portrait are typical for a T^2 torus (see Fig. 13d), typical for a quasi-periodic state. The analysis of a time-series taken near the cathode, much more corrupted with noise, leads to less clear results.

Increasing the discharge current leads to a destruction of the quasi-periodic regime and to a more and more complex spatiotemporal behavior. Beyond the chaotic regime $I = 76$ mA displayed in Figure 11a there is a lost of spatial coherence.

The analysis of the regime depicted in Figure 12a shows that it is due to a strongly developed spatiotemporal chaos of ionization waves with a broad frequency spectrum. The high values of the dimensions obtained for this regime lead to the evidence that the regime is indeed turbulent. The lack of value for the cathode side correlation dimension (Tab. 4) is due to the fact the convergence required in order to determine the dimensionality was not achieved.

The weights distribution and the quantity $D_{\mathrm{BD}}(K)$ from the biorthogonal decomposition of the spatio-temporal signals are shown in Figure 14.

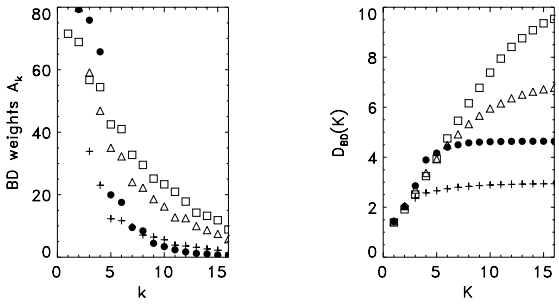

(a) (b)

Fig. 14. Limit cycle (•), quasi-periodic (+), chaotic (△), and turbulent (□) regimes; (a) weights distribution, (b) $D_{\mathrm{BD}}(K)$.

As previously, a possible saturation of the quantity $D_{\mathrm{BD}}(K)$ plotted in Figure 14b indicates whether the spatiotemporal dynamics is adequately described by only a few dominating modes.

It is interesting to note that for the limit cycle regime it is not possible to separate the space-time structure into two different propagating waves. This is typical for a synchronized state which builds up from two interacting waves having commensurate frequencies, (see [10]). The reconstruction of the space-time structure from the BD needs to add the first four modes (see Figs. 15a and 15b). The spatiotemporal complexity of this regime is thus higher than in the quasi-periodic regime, as it reflects in the behavior of the quantity $D_{\mathrm{BD}}(K)$ as depicted in Figure 14b.

As in the case of the sub-harmonics cascade, the stability of the mode associated with the coefficients (α_1, α_2) is clearly seen in Figures 15c and 15d, while the modes associated with the other dominating coefficients change during the transition towards turbulence.

The weights distribution and the quantity $D_{\mathrm{BD}}(K)$ for the turbulent regime are very different compared to the case of the periodic, quasi-periodic and chaotic regimes. Indeed, the quantity $D_{\mathrm{BD}}(K)$ does not saturate in this case. A maximal value L of the number K greater than the actual value ($K_{\max} = 16$), *i.e.*, number of photo-diodes, would be needed to get the saturation of the quantity $D_{\mathrm{BD}}(K)$.

According to this analysis, the physical mechanism seems to be the following: the cathodic region of the discharge behaves as an oscillator whose frequency varies with the discharge current. This behavior has also been shown previously for a glow discharge in a closed sealed tube [16,17]. This oscillator excites an ionization wave in the region of the positive column near to the cathode. The frequency of the wave is naturally identical to that of the oscillator. This first mode excited by the cathode oscillation is the only propagating from the cathode up to a distance, about equal to the optimal wavelength in the operating discharge conditions. But starting from this distance a nonlinear mechanism of parametric excitation takes place, and excites the dominating mode of the positive column together with its harmonics. The quasi-periodicity route thus results from the respective evolution of the two modes with the discharge current.

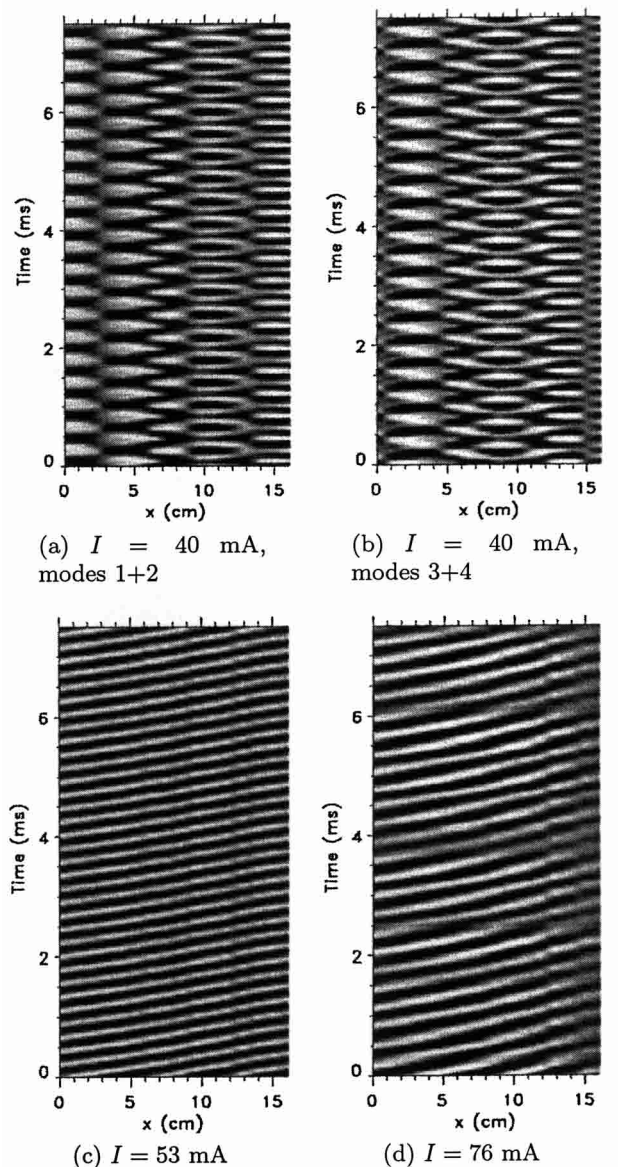

Fig. 15. Space-time dynamics of the dominant modes $\sum_{k=p}^{k=q} \alpha_k \Psi_k(t_i)\Phi_k(x_j)$, with $p = 1$ and $k = 2$ (except for (b)), reconstructed from the biorthogonal decomposition of space-time data from: (a) synchronized , (b) same as (a) but with $p = 3$, $q = 4$, (c) quasi-periodic, and (d) chaotic regimes.

3.3 Low current

In addition to the transitions towards chaos already mentioned (sub-harmonics cascade or RTN scenario), a transition towards complexity by intermittency can also be observed. This situation is obtained at a fixed value of the control parameter. The dynamical regime of the discharge changes transiently without any external action on

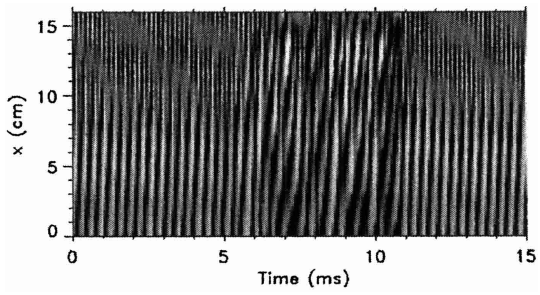

Fig. 16. Intermittent regime of ionization waves. The anode is on bottom and the cathode on top.

the parameters of the system. The regular motion of the discharge is then intersected with irregular puffs.

In Figure 16 a spatiotemporal signal of a regular evolution intersected by irregular bursts is displayed (gray-level image and time-series). This has been obtained for the product $pR = 7.2$ cm torr and a discharge current of 32 mA. It is suspected that crisis-induced intermittency [18] is present in this regime. The examination of the space-time signals of the intermittent regimes reveals that the transition is initiated by a local disturbance.

The spatial structure of the signal plays a significant role in the appearance of the chaotic bursts, since these initially weak local disturbances are growing along the positive column. They are the trigger mechanism for phase and amplitude defects. Moreover, the transition towards ionization waves chaos in the discharge can be a mixture of one of the scenarios described above and intermittency, because the intrinsic fluctuations of the plasma which lead to the intermittent behavior can occur in any dynamical regime of the discharge.

4 From a compact system to an extended dynamical system

The transition from a small compact dynamical system to a large dynamical system by changing the spatial extent is of high interest. A spatial extent is the necessary condition for the occurrence of spatiotemporal chaos and weak turbulence. In our case, the grounded anode is movable along the tube and the length of the positive column can be varied from a few centimeters to 80 cm. Three situations have been can observed according to the discharge length:

- short discharge: the length of the positive column is lower than the typical wavelength (about 13 cm) of the ionization waves. The transition towards chaos is obtained following the sub-harmonics route. But as compared to the situation depicted in Section 3.1 the classical period doubling scenario is observed. The period of the fluctuations is the same one along the plasma column. The system is compact. It behaves as a nonlinear unstable oscillator with purely temporal dynamics;

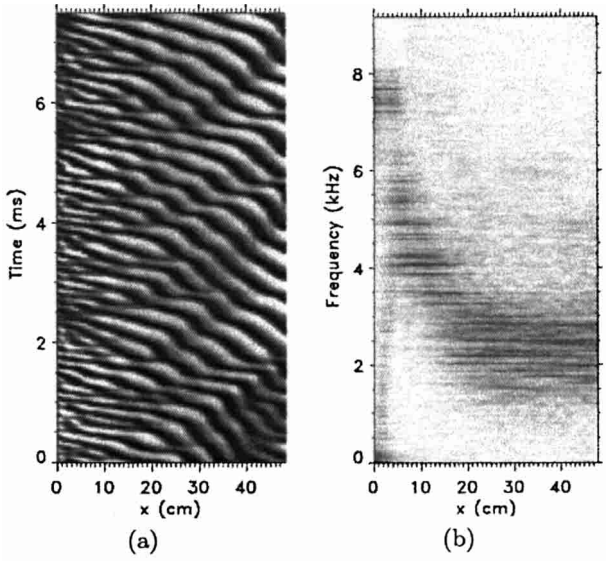

Fig. 17. Long discharge. Space-time (a) and space-frequency (b) images.

- intermediate lengths: when the discharge length is about three times the typical wavelength of the unstable waves, the three scenarios previously described can be observed. The system is no longer compact;
- eventually, if the discharge has a length larger than approximately three times the maximum wavelength of the fundamental ionization waves, spatio-temporal chaos is observed all along the plasma column whatever the discharge current.

The situation where the discharge can be regarded as a large dynamical system is illustrated in Figure 17. The spatiotemporal signal represented on this figure was obtained using forty-eight optical detectors located along the plasma column. It is worth noting that the phase velocity of the ionization waves fluctuates along the column and that the dynamics is chaotic both in time and space.

5 Conclusion

Analysis of experimental space-time data using classical tools and the biorthogonal decomposition as well, permit us to characterize the spatio-temporal dynamics of ionization waves self-excited in a glow discharge plasma. Three different transition scenario, *i.e.*, sub-harmonics cascade, Ruelle-Takens-Newhouse scenario, and intermittence, have been identified, that lead from periodic regular regimes to chaos and turbulence of ionization waves. The difference in the dynamical regime between the anode and cathode sides of the discharge have been pointed out by the spatio-temporal analysis of the fluctuations of the light emission along the plasma column. The transition from a compact system to an extended one has been investigated as well.

The next step of trying to understand the non linear interaction between the fundamental wave of the positive

column and the wave launched from the cathode end is under way.

The authors are very much indebted to J.-L. Briançon for programming of the signal acquisition units and J.-F. Pautex, Ch. Thiebaut, A. Fleuret for technical assistance.

References

1. M.C. Cross, P.C. Hohenberg, Rev. Mod. Phys. **65**, 851 (1993).
2. N.L. Oleson, A.W. Cooper, Adv. Electron. Electron. Phys. **24**, 155 (1968).
3. L. Pekárek, J. Krása, *Proc. of 7th Yugoslav Symposium and Sum. Sch. on the Phys. of Ion. Gaz*, edited by V. Vujnovic, pp. 915-957 (1974).
4. P.S. Landa, N.A. Miskinova, Yu.V. Ponomarev, Sov. Phys. Usp. **23**, 813 (1980).
5. K.-D. Weltmann, H. Deutsch, H. Unger, C. Wilke, Contrib. Plasma Phys. **33**, 73 (1993).
6. K. Ohe, Curr. Top. Phys. Fluids **1**, 319 (1994).
7. N. Aubry, R. Guyonnet, R. Lima, J. Nonlin. Sci. **2**, 249 (1992).
8. P. Holmes, J. Lumley, G. Berkooz, J. Mattingly, R. Wittenberg, Phys. Rep. **287**, 337 (1997).
9. T. Dudok de Wit, R. Lima, A.-L. Pecquet, J.-C. Vallet, Phys. Plasmas **1**, 3288 (1994).
10. A. Atipo, X. Caron, G. Bonhomme, T. Pierre, C.R. Acad. Sci. Paris **327**, Série II b, 259 (1999).
11. H.D. Abarbanel, *Analysis of observed chaotic data* (Springer, New-York, 1995).
12. H. Kantz, T. Schreiber, *Nonlinear Time Series Analysis* (Cambridge University Press, Cambridge, 1997).
13. P. Grassberger, I. Procaccia, Phys. Rev. Lett. **50**, 346 (1983).
14. M. Sano, Y. Sawada, Phys. Rev. Lett. **55**, 1082 (1985).
15. T. Kruel, M. Eiswirth, F. Schneider, Physica D **63**, 117 (1993).
16. A. Dinklage, P. Jonas, C. Wilke, G. Bonhomme, A. Atipo, *Proc. of the 1998 ICPP* and *25th EPS Conf. on Controlled Fusion and Plasma Physics*, Praha, contributed papers (1998).
17. A. Dinklage, C. Wilke, G. Bonhomme, A. Atipo, Phys. Rev. E **62**, 7219 (2000).
18. C. Grebogi, E. Ott, J.A. Yorke, Phys. Rev. Lett. **48**, 1507 (1982).